Perth-Muenster REG-REG correlations
Remarkable new evidence for dynamical space

Peter C. Morris

Adelaide, South Australia. May 21, 2018

E-mail: ptr.mrrs@tpg.com.au

We have obtained new evidence for dynamical space by applying correlation analysis to a year of data from a Random Event Generator (REG) device located in Perth, Australia and from another in Muenster, Germany, recorded between July 1, 2012 and June 30, 2013. The results obtained are consistent with results obtained by applying similar analysis to data from a REG located in Manchester UK and the REG in Perth. Consequently evidence for dynamical space is mounting.

For each day we applied correlation analysis to determine travel times for putative waves. Then wave speed and direction, over each 24 hour period, were determined by fitting to the observed travel times, theoretical curves of how travel times would vary with Earth rotation. We thereby derived an average incoming RA, declination and speed for the waves of each day.

A probability density plot of the incoming directions exhibited a peak near $RA = 4.5\,h$, consistent with previous determinations of incoming space flow direction by Reginald Cahill and Dayton Miller. Moreover, removing Earth orbital and gravitational inflow velocities from the observed wave velocities allowed a peak of higher density to be obtained, which is consistent with predictions of Dynamical 3-Space theory. The peak indicated a most probable incoming galactic direction of $RA = 4.50\,h$, $dec = -80.6\,deg$. Probability density plots of speeds indicated a most probable incoming galactic speed of $502\,km/s$.

1 Dynamical 3-space waves

In Cahill's theory of Dynamical 3-Space [1,2], gravity is caused by acceleration of space into matter. The flow equations governing this process are nonlinear and nonlocal and when applied to translation of matter through space, while space is concurrently accelerating into matter, predict generation of fluctuations and waves within the flow fields [5].

Random Event Generator (REG) devices commonly generate random numbers by detecting the quantum to classical transition of electrons tunnelling through a barrier in a Zener diode. In the standard interpretation of quantum theory such transitions were assumed to be completely random, however Cahill's theory and experiments [1] suggest that this is not the case and that the transitions are driven by the aforementioned fluctuations and waves in 3-space. If so, then the potential presence of waves within passing space implies that the numbers output by two spatially separated REG devices may not be 100% independent and that correlation analysis of data from the devices could potentially reveal the travel time of waves that influenced both devices.

To test this possibility we have been analysing data from Global Consciousness Project [8] REG devices. Herein we describe results from a REG located in Perth, Australia and from another in Muenster, Germany, as shown in Table 1 for all days for which data was available, from 1 July 2012 to 30 June 2013.

Of 365 potential days data was available for 198.

Table 1: Details of GCP REG Devices Used

	Perth	Muenster
ID Number	2232	3023
Latitude	-31.921	52.267
Longitude	115.892	8.05
Device Type	Orion	Orion

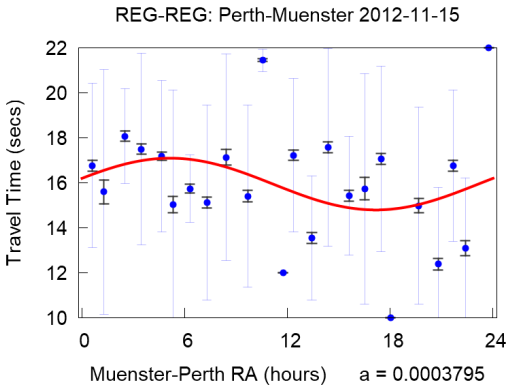

Fig. 1: Travel times from Perth to Muenster from REG-REG data for November 15, 2012. High correlation values for each Muenster-Perth RA hour have been binned and the mean, SD (blue) and SEM (grey) shown. The red curve shows a least square error best fit of a sinusoid to all points. (Horizontal spacing of points is non-uniform because the RA of each point is the mean RA of values in the associated bin).

2 Travel times

For each of the 198 days for which data was available, Perth to Muenster travel time τ values were determined by computing the correlation function,

$$C(\tau, t) = \sum_{t'=t-T}^{t'=t+T} S_1[t' - \lfloor \tau/2 \rfloor] \, S_2[t' + \lceil \tau/2 \rceil] \, e^{-a(t'-t)^2} \tag{1}$$

for data sequences $S_1[t]$ and $S_2[t]$ containing values output once per second by the REG devices. Here $\lfloor \rfloor$ and $\lceil \rceil$ represent floor and ceiling functions that round $\tau/2$ down or up to integer values to ensure correct indexing when τ is an odd number. $2T = 300s$ is the time interval used about UTC time t, and the Gaussian term applies a Gaussian window to suppress end effects. The width of this window is controlled by parameter a chosen as described in the following section.

τ values were determined by calculating $C(\tau, t)$ for τ in the range 9 to 23 seconds and then finding which value of τ in the range 10 to 22 corresponded to the maximum peak value of $C(\tau, t)$.

τ values with high correlations* were then binned and averaged per RA hour of the Muenster-Perth spatial separation vector that rotates with the Earth. We thereby obtained a mean travel time, Standard Deviation (SD) and Standard Error in the Mean (SEM) for 24 RA directions such as shown in Fig. 1.

*For each day the high correlations were all those higher than a cutoff value which would allow each bin to contain at least one sample. To the bin(s) which then contained only one sample, a second sample with the nearest slightly lower correlation was added to allow calculation of standard deviation.

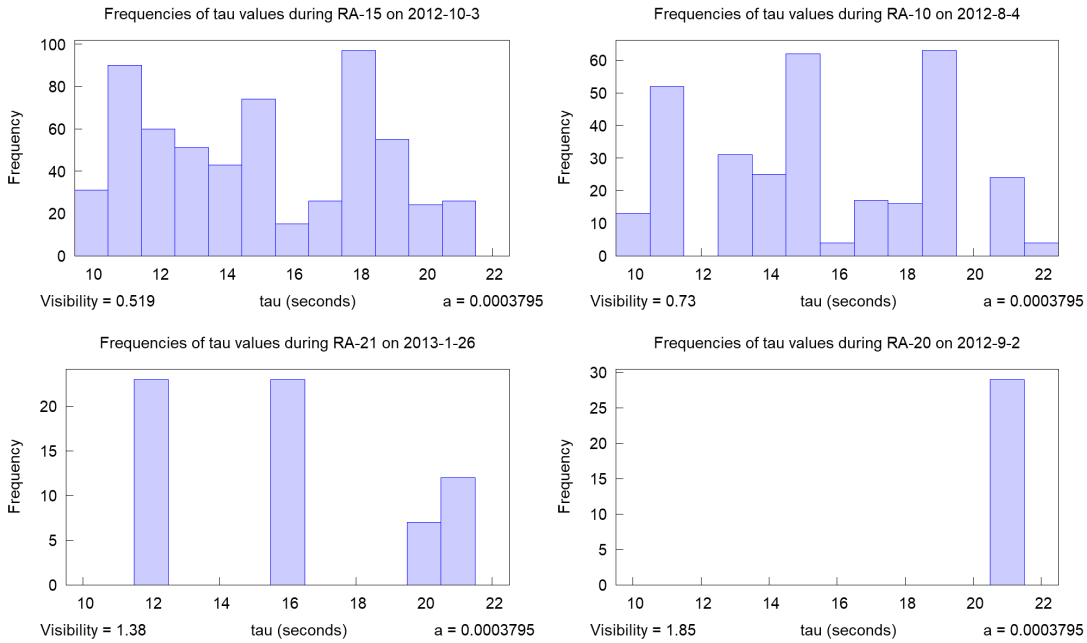

Fig. 2: Histograms of Perth-Manchester τ values detected during different RA hours illustrating a range of signal visibilities from low to high. The multiple peaks are consistent with passage of non-distinguishable waveforms, $w_n, w_{n+1}, w_{n+2}...$ etc. three to five seconds apart. Then the correlation of w_n at one detector with say w_{n+1} or w_{n+2} at the other, may be as large as the correlation with w_n. The single peak in the last histogram is consistent with passage of distinguishable waveforms.

3 Gaussian window parameter a

For Gaussian window parameter a we used a value of 0.0003795 which we had earlier determined as optimum when determining travel times between the REG in Perth and a REG located in Manchester, UK. [3]. As this value also worked well for the Perth-Muenster REG-REG combination, we did not try to determine a better value for Perth-Muenster.

However, for Perth-Manchester we had proceeded as follows.

First, we binned τ values to obtain histograms such as shown in Fig. 2 and applied the following notion of signal visibility.

Let bar heights $y_1, y_2 \ldots y_N$ be the frequencies of τ values in columns $1, 2 \ldots N$. Then we can define signal visibility as mean deviation of bar height over mean bar height, ie.,

$$V(y) = \frac{\frac{1}{N}\sum_{i=1}^{N} |y_i - \bar{y}|}{\bar{y}} \tag{2}$$

Applying this formula to a histogram containing equal numbers of bars with heights equal to max and min gives,

$$V = \frac{max - min}{max + min}$$

which is the formula for signal visibility used in interferometry. However, whereas the latter has a maximum value of $V = 1.0$ when $min = 0$, Eqn. (2) gives higher values when the number of maxima is reduced. Eg if a histogram contains one bar of height equal to max and $(N-1)$ with height of zero, then for our histograms with 13 bars (2) gives,

$$V(y) = 2\frac{N-1}{N} \approx 1.85$$

Using (2) we determined minimum visibility for each day and then the mean minimum for all days for a range of a values. The blue curve in Fig. 3. shows results obtained from Perth-Manchester data from seven days centered on each full moon during a year. This has a distinct peak at $a = 0.0003795$ so we used this value of a for subsequent calculations.

The red curve shows the mean for all days of the median standard error per day in the hourly τ values. This increases with a because increasing a reduces the width of the Gaussian window and reduces the number of correlation products that are averaging together, however the rate of increase shows a slight leveling off at peak visibility.

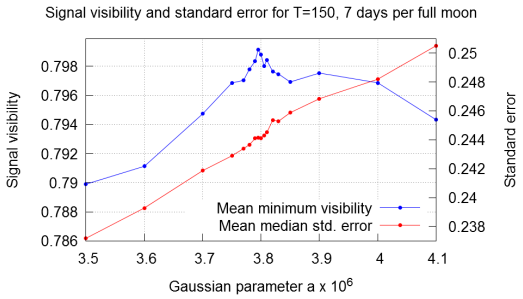

Fig. 3: Plots earlier obtained [3] from Perth-Manchester data of mean minimum signal visibility and mean median travel time standard error for 7 days per each full moon during a year versus Gaussian window parameter a. The peak visibility occurred at $a = 0.0003795$.

4 Wave effects in histograms

The histograms of τ values shown in Fig. 2, earlier obtained for Perth-Manchester travel times, illustrate a range of signal visibilities obtained during different RA hours. Histograms often had multiple peaks consistent with passage of similar waveforms, $w_n, w_{n+1}, w_{n+2}...$ etc. three to five seconds apart and which may have changed shape during passage from one REG to the other. Then the correlation of w_n at one detector with say w_{n+1} or w_{n+2} at the other, could be as large or larger than correlation with w_n. The presence of multiple peaks resulted in mean τ values with large standard deviations and also caused variation of the mean values to be attenuated towards the center of the 10 to 22 second detection range. To compensate for this we applied a disattenuation procedure to derived results as described later.

5 Fitting of sinusoids

Given travel time data for 24 RA directions, the incoming speed and the direction of plane waves can be determined by fitting,

$$\tau = \frac{\mathbf{R} \,.\, \mathbf{v}}{\mathbf{v}^2} \tag{3}$$

where $\mathbf{R}$ is the REG-REG spatial separation vector and $\mathbf{v}$ is the velocity of the Earth relative to the waves. As the daily rotation of $\mathbf{R}$ causes the right hand side of Eqn. (3) to be sinusoidal, the fit can be done by fitting a sinusoid to the travel times such as shown in Fig. 1.

The RA of the peak will then indicate the incoming RA of the waves and the amplitude and mean will allow determination of incoming declination and speed. However, the means and amplitudes need to be adjusted to compensate for the above mentioned attenuation effect.

6 Amplitude disattenuation

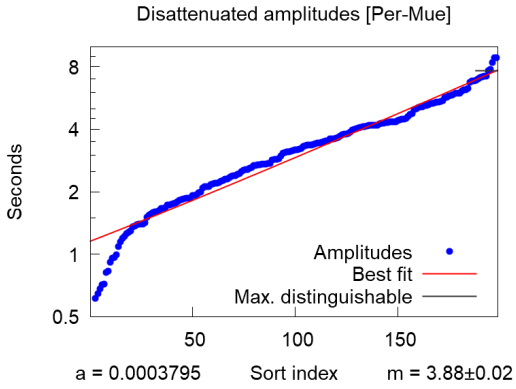

Fig. 4: Disattenuated amplitudes obtained from Perth-Muenster travel times by sorting the original values and then multiplying by a suitable value m to allow the best fit exponential curve to match the range of the detection process. Here use of a logarithmic vertical axis results in a straight line plot.

When τ values obtained during a given RA hour are averaged together, the presence of multiple peaks in histograms such as seen in Fig. 2 implies that wrong values caused by miscorrelation will be averaged together with correct values and the resultant mean value is then likely to be attenuated towards the center of the detection range. If we assume such wrong values have a random distribution within the observation window, this phenomenon will cause the amplitudes of the sinusoids to be attenuated by an amount equal to $1/(1+n)$ where n is the average number of miscorrelation values per correct τ value.

To compensate for this effect we multiplied the sinusoid amplitudes so that a best fit of an exponential curve to a sorted list of the multiplied values terminated at the amplitude of the largest sinusoid that could be fit to a waveform clipped to the τ range of 10 to 22. This "largest distinguishable amplitude" is 7.66. The exponential fit is shown in Fig. 4, where a logarithmic vertical axis makes it appear as a straight line plot. This resulted in a multiplier of $m = 3.88 \pm 0.02$.

It can be noted that this value corresponds to $n = (m-1) \approx 2.9$ miscorrelation values per correct value.

7 Incoming declination and speed

If we let τ_{mean} and τ_{amp} be the mean and amplitude of each sinusoid fit, τ_{mid} be the center of the detection range and m be the disattenuation multiplier determined above, then the disattenuated mean value will be,

$$T_{mean} = \tau_{mid} + m(\tau_{mean} - \tau_{mid})$$

and the disattenuated amplitude will be $A = m\tau_{amp}$ and we can define,

$$T_{max} = T_{mean} + A$$

$$T_{min} = T_{mean} - A$$

Then if $\delta_{\mathbf{R}}$ and $\delta_{\mathbf{v}}$ are respectively the declinations of $\mathbf{R}$ and $\mathbf{v}$, then $\delta_{\mathbf{v}}$ can be found by numerically solving,

$$\frac{T_{min}}{T_{max}} = -\frac{cos(\delta_{\mathbf{v}} + \delta_{\mathbf{R}})}{cos(\delta_{\mathbf{v}} - \delta_{\mathbf{R}})} \tag{4}$$

And wave speed relative to Earth is then,

$$s = \frac{|\mathbf{R}|\, cos(\delta_{\mathbf{v}} - \delta_{\mathbf{R}})}{T_{max}} \tag{5}$$

8 Aberration of incoming wave velocity

Let $\mathbf{v}_G$ be the velocity of the Sun relative to distant galactic space, $\mathbf{v}_{inS}$ be velocity due to acceleration of space towards the Sun, $\mathbf{v}_{orbit}$ be the orbital velocity of the Earth and $\mathbf{v}_{inE}$ be velocity due to acceleration of space towards the Earth. Then the velocity of a point on or within Earth relative to incoming 3-space can be approximated by,

$$\mathbf{v} \approx \mathbf{v}_G - \mathbf{v}_{inS} + \mathbf{v}_{orbit} - \mathbf{v}_{inE} \tag{6}$$

Approximate vector addition of these components is possible because at the Earth's orbital positions, $\mathbf{v}_G$, $\mathbf{v}_{inS}$ and $\mathbf{v}_{orbit}$ are approximately orthogonal and $\mathbf{v}_{inE}$ represents a relatively small Earth directed effect. (Justification for vector addition of the first three components can be found in [5].)

From (6) it follows that if 3-space waves have a constant velocity relative to space and if $\mathbf{v}_{WG}$ is the velocity of the Sun relative to distant waves, then the velocity of a point on or within the Earth relative to incoming waves is,

$$\mathbf{v}_W \approx \mathbf{v}_{WG} - \mathbf{v}_{inS} + \mathbf{v}_{orbit} - \mathbf{v}_{inE} \tag{7}$$

which expresses how wave velocities are aberrated by the orbital and inflow velocities.

However the speeds that we derive from T_{max} in (5) correspond to *average* speeds of waves through deep paths through the Earth. Calculation of such speeds for the expected range of values of $\mathbf{v}_{WG}$, showed that the effect of higher speeds induced by $\mathbf{v}_{inE}$ along the downward portions of such a paths, would be almost exactly cancelled by the effect of lower speeds induced along the upward portions.

This implies that for average travel time velocities $\mathbf{v}_{Wtt}$, derived from travel times through the Earth, we will have,

$$\mathbf{v}_{Wtt} \approx \mathbf{v}_{WG} - \mathbf{v}_{inS} + \mathbf{v}_{orbit} \tag{8}$$

ie. without the $\mathbf{v}_{inE}$ term.

Then to remove the aberrating velocities and obtain $\mathbf{v}_{WG}$ from $\mathbf{v}_{Wtt}$ we can rearrange (8) as,

$$\mathbf{v}_{WG} \approx \mathbf{v}_{Wtt} + \mathbf{v}_{inS} - \mathbf{v}_{orbit} \tag{9}$$

9 Probability density plots of wave direction

Using the methods described above we calculated an incoming RA, declination, speed and associated standard deviations, for each of the 198 days for which data was available.

Fig. 5 shows a probability density plot of incoming directions for all days with a highest peak near $RA = 3.0\,h$ and a lower peak near $RA = 18\,h$.

However, if the velocities contributing to the main peak are of physically real waves per dynamical 3-space theory, then they should have been aberrated by Earth orbital and Sun inflow velocities and so

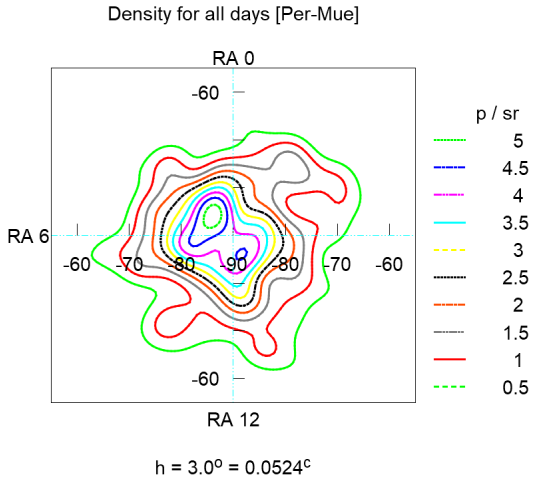

Fig. 5: Probability density of incoming wave directions for all days. (p/sr means probability per steradian and h is the bandwidth of the Gaussian kernel.)

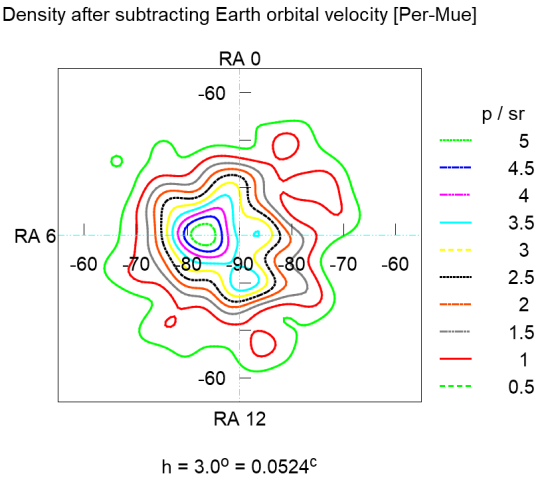

Fig. 6: Probability density after removing Earth orbital velocity.

removing these velocities from the observed wave velocities should result in a higher and more dominant peak.

This turns out to be the case.

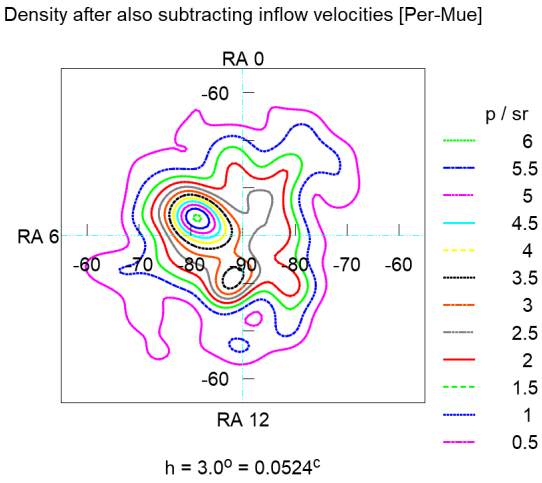

Fig. 7: Probability density after removing Earth orbital and Sun inflow velocities.

Fig. 6 shows that removing Earth orbital velocity results in a more dominant highest peak and Fig. 7 shows that removing the Sun inflow velocity as well as the Earth orbital velocity results in an even higher and more dominant peak near $RA = 4.5\,h$.

By applying a search procedure to find the peak of Fig. 7, the highest probability density was found to be 6.11 at $RA = 4.50\,h$, $dec = -80.6^0$.

We take the above direction as our best estimate of the direction of $\mathbf{v}_{WG}$ which we have defined as the velocity of the Sun relative to distant galactic waves. In the next section we will derive the speed.

10 Probablity density plots of wave speed

In the previous section we described removal of orbital and inflow velocities from incoming wave velocities so as to obtain galactic wave velocities, ie., the incoming velocities that the waves would have had relative to the sun, when very distant from the solar system.

Fig. 8 shows plots of probability density versus speed for all waves irrespective of incoming direction.

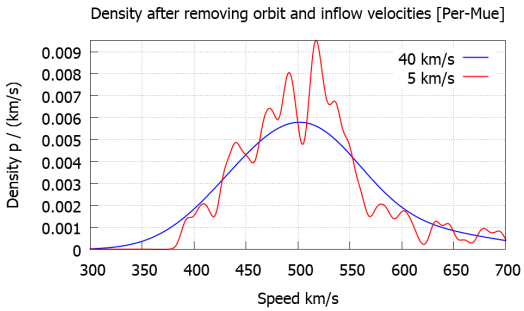

Fig. 8: Probability density plots of galactic wave speed for all incoming waves.

The plots show results for two different speed bandwidths. The blue curve is for a bandwidth of $40\,km/s$. This is wide enough to give a simple to interpret, smooth curve, with a single peak at $502\,km/s$. We take this as our best estimate for average wave speed $|\mathbf{v}_{WG}|$.

The red curve with a bandwidth of $5\,km/s$ has a minimum at this speed with two main peaks either side. A possible cause of this pattern is that speeds varied in a periodic manner such that at our sampling rate of one sample per day only a few samples were obtained per cycle. Then the relative phase of the sampling could have caused samples to have been more frequently obtained either side of the average speed, than at or near the average speed. If this is the case, re-sampling with a different phase (by refitting the daily sinusoids), might result in a different pattern.

Alternatively, the peaks might represent waves travelling in opposite directions relative to space.

11 Confidence interval estimation

To estimate confidence intervals for the RA and declination of the peak density shown in Fig. 7, we applied bootstrap resampling [9] to the 198 wave directions. To do this we repeatedly made a random selection of 198 directions from the original 198 and then found the peak density for this random set.

Repeatedly applying this procedure gave multiple estimates of RA and declination from which we calculated 68.3% confidence intervals. Fig. 9 shows an example of results obtained from two thousand iterations.

This allowed us to calculate $RA = 4.50^{+0.32}_{-0.19}\,h$ and $dec = -80.6^{+0.9}_{-1.4}\,deg$.

Applying a similar procedure to wave speed, gave $502^{+5}_{-6}\,km/s$ for the blue peak in Fig. 8.

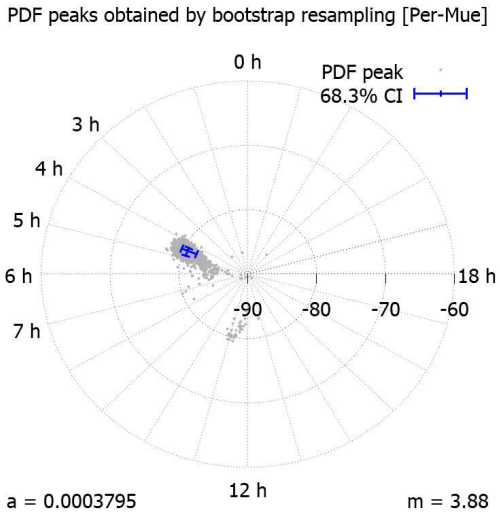

Fig. 9: Example of 2000 iterations of bootstrap resampling. Each point shows a peak of probability density calculated from a different set of 198 wave directions randomly selected from the 198 available directions.

12 RA probability calculation

Having obtained an estimate of $\mathbf{v}_{WG}$, we can use Eqn. (8) to predict probable values of incoming wave direction and speed $\mathbf{v}_{Wtt}$ that would be observed by the Perth-Muenster REG detectors as Earth orbital and Sun inflow velocities vary during a year. The red curve in Fig. 10 shows predicted RA while the points show the RAs of the observed 198 incoming wave velocities.

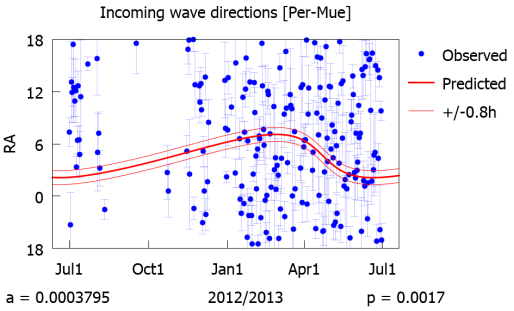

Fig. 10: Points show the RAs of the 198 incoming wave directions. The red curve shows RA values obtained from Eqn. (8) using our estimate of $\mathbf{v}_{WG}$ with $RA = 4.50\,h$, $dec = -80.6^0$ and $speed = 502\,km/s$. Of 198 points, 25 lie within ± 0.8 RA hours of this curve. The probability of this degree of closeness arising from chance is $P_{RA} = 0.0017$.

Inspection of Fig. 10 reveals that 25 of the 198 points lie within ± 0.8 RA hours of predicted RA. However if the RAs were random, axial symmetry would imply a uniform distribution and we would expect only $198 \times \frac{1.6}{24} = 13.2$ points to lie this close to the curve.

We then checked the probability of the observed distribution being due to chance using the formula,

$$P = \sum_{k=r}^{n} \binom{n}{k} p^k (1-p)^{n-k} \tag{10}$$

where $r = 25$ is the number of points within ± 0.8 RA hours of the curve, $n = 198$ is the total number

of points and $p = 1.6/24$ is the probability of a point lying within ± 0.8 RA hours of the curve if the distribution of RAs was random and uniform.

Inserting these figures gives $P_{RA} = 0.0017$.

13 Declination probability calculation

Since the derivations of the declinations and RAs are mutually independent, we can validly make an independent check of the probability of the derived declinations. The points in Fig. 11 show the 25 incoming wave directions whose RAs in Fig. 10 were within $\pm 0.8\,h$ of predicted RA. The blue orbital aberration ellipse shows predicted RA and declination over the course of a year calculated using Eqn. (8) with our estimate of $\mathbf{v}_{WG}$.

Of 25 points, the 20 shown as solid have declinations that lie within $\pm 7.01^0$of the predicted values.

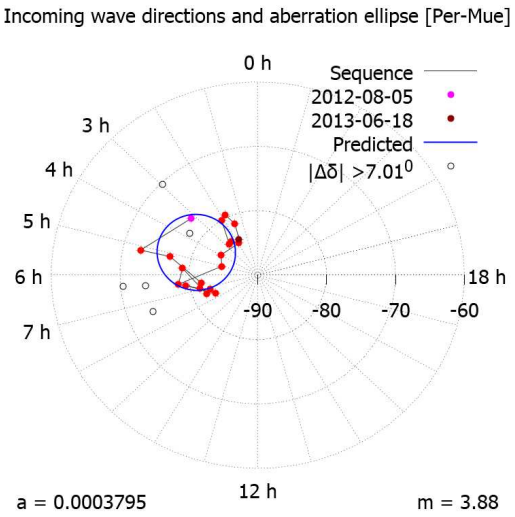

Fig. 11: Points show the 25 incoming wave directions whose RAs in Fig. 10 are within $\pm 0.8\,h$ of predicted RA. The blue orbital aberration ellipse shows variation of predicted RA and declination during a year due to the combined effect of Earth orbital and Sun inflow velocities. Of the 25 points, 20 shown as solid have declinations that lie within $\pm 7.01^0$of predicted values. The probability of this closeness being a result of chance is $P_{dec} = 2.0 \times 10^{-4}$.

This prompts the question, "If the declinations of the points were selected at random from the distribution of declinations that we would have obtained if our data was random, what is the probability that 20 out of 25 would lie this close to their predicted declination?"

To answer this, we first calculated a declination empirical cumulative distribution function (ECDF) by repeatedly applying our code to randomized travel time values and recording the simulated declinations obtained. Fig. 12 shows the results for 30×365 such declinations.

Then for each of the 20 points, we used the distribution function to calculate the probability that a declination drawn at random from the distribution would be as close as observed to the predicted value. We then took the maximum probability as a conservative probability for all 20 points. This maximum probability turned out to be 0.4324 and was for a maximum deviation of $\pm 7.01^0$

We could then reapply Eqn. 10 where this time $r = 20$ is the number of points with declinations within $\pm 7.01^0$ of their predicted value, $n = 25$ is the total number of points and $p = 0.4324$ is the maximum probability of a point having a declination within ± 7.01 of its predicted value if its declination was drawn at random from the above distribution.

Inserting these figures gives $P_{dec} = 2.0 \times 10^{-4}$.

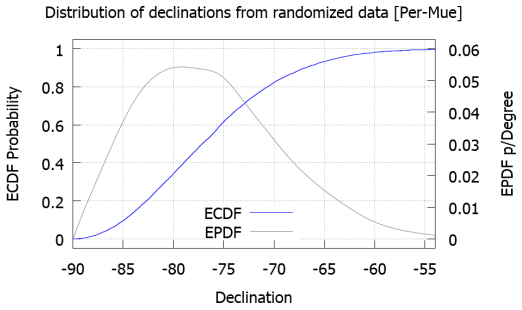

Fig. 12: Blue curve shows empirical cumulative distribution function for declinations derived from randomized travel times. That is, for each RA of each day to be simulated, a travel time was selected at random from the set of 24×198 travel times that had been determined for the 198 days that had complete data. Gray curve shows the corresponding empirical probability distribution function.

14 Joint probability

Since the RAs and declinations were independently derived, the joint probability that the closeness of their observed values to their predicted values could have arisen by chance is $P = P_{RA} \times P_{dec} = 0.0017 \times 2.0 \times 10^{-4}$, which gives,

$$P = 3.4 \times 10^{-7}$$

15 Comparison with related results

Table 2 shows a comparison between values of galactic wave velocity $\mathbf{v}_{WG}$ reported in this and earlier papers [3, 4] by this author and values of galactic space flow velocity $\mathbf{v}_G$ reported by Cahill in [6, 7].

Table 2: Comparison of related results

Ref.	Source of data		RA (hrs)	dec (deg)	speed (km/s)
This paper	REG-REG Perth-Muenster	$\mathbf{v}_{WG}$	$4.50^{+0.32}_{-0.19}$	$-80.6^{+0.9}_{-1.4}$	502^{+5}_{-6}
Morris [3]	REG-REG Perth-Manchester	$\mathbf{v}_{WG}$	$4.13^{+0.83}_{-0.81}$	$-77.8^{+2.7}_{-2.1}$	505^{+11}_{-8}
Morris [4]	REG-REG Perth-Manchester	$\mathbf{v}_{WG}$	4.00 ± 0.51	-79.8 ± 1.0	500 ± 113
Cahill [6]	NASA spacecraft doppler radar	$\mathbf{v}_G$	4.29	-75	486
Cahill [7]	Miller gas mode interferometer	$\mathbf{v}_G$	5.2	-67	433

16 Conclusions

In this paper we have presented results that illustrate correlations between widely separated Random Event Generator devices in Perth, Australia and Muenster, Germany that appear to be caused by waves of cosmic origin that are aberrated by Earth orbital and Sun inflow effects, while approaching Earth at

some $500\,km/s$. Our analysis and probability calculations show that it is very unlikely ($P < 4.0 \times 10^{-7}$) that the observed correlations could have occurred as a result of chance alone. In an earlier paper [3] we reported similar results with $P < 6.7 \times 10^{-5}$ after applying correlation analysis to data obtained from a REG located in Manchester UK and the REG in Perth.

Consequently evidence for the wave phenomenon seems strong. To interpret and analyse our data we applied Cahill's theory of dynamical 3-space. This allowed us to obtain intelligible results consistent with the theory and currently seems the best available explanation for what we have observed.

Acknowledgements

Special thanks are owed to GCP [8] and its director Dr. Roger Nelson for enabling access to valuable data from the GCP network of REG devices.

Thanks to Pierre Millette for insightful suggestions with respect to earlier work leading to this paper.

References

[1] R.T. Cahill, Nanotechnology Quantum Detectors for Gravitational Waves: Adelaide to London Correlations Observed. *Progress in Physics*, 2013, v. 4, 57-62. http://www.ptep-online.com/2013/PP-35-09.PDF

[2] R.T. Cahill, Discovery of Dynamical Space: Experiments and Theory, Proc. SPIE 9570, *The Nature of Light: What are Photons?* VI, 957018 (September 10, 2015) http://dx.doi.org/10.1117/12.2188802

[3] P.C. Morris, Evidence for Cahill's Dynamical Space, http://vixra.org/pdf/1703.0250v4.pdf

[4] P.C. Morris, Estimating 3-Space Velocity from REG-REG Correlations, http://vixra.org/pdf/1604.0352v3.pdf

[5] R.T. Cahill, The dynamical velocity superposition effect in the quantum-foam theory of gravity, *Relativity, Gravitation, Cosmology: New Developments*, Dvoeglazov V., ed., Nova Science Pub., New York, 113-131, 2010. http://arxiv.org/pdf/physics/0407133.pdf

[6] R.T. Cahill, Combining NASA/JPL one-way optical-fiber light-speed data with spacecraft Earth-flyby Doppler-shift data to characterise 3- space flow, *Progress in Physics*, 2009, issue 4, 50-64. http://www.ptep-online.com/2009/PP-19-05.PDF

[7] R.T. Cahill, Process Physics, *Process Studies Supplement Issue 5, 1-131(2003)* The Center for Process Studies http://www.mountainman.com.au/process_physics/HPS13.pdf

[8] The Global Consciousness Project http://global-mind.org/

[9] T. Hesterberg, What Teachers Should Know About the Bootstrap: Resampling in the Undergraduate Statistics Curriculum *Am Stat.* 2015 Oct 2; 69(4): 371–386.

[10] R.N. Bannister, A guide to computing orbital positions of major solar system bodies: forward and inverse calculations http://www.met.rdg.ac.uk/%7Eross/Documents/OrbitNotes.pdf http://www.met.rdg.ac.uk/%7Eross/Astronomy/Planets.html

[11] D.C. Miller, The Ether-Drift Experiment and the Determination of the Absolute Motion of the Earth *Rev. Mod. Phys.* 5, 203 – Published 1 July 1933.